



HAL
open science

On the development of an original mesoscopic model to predict the capacitive properties of carbon-carbon supercapacitors

Anouar Belhboub, El Hassane Lahrar, Patrice Simon, Céline Merlet

► To cite this version:

Anouar Belhboub, El Hassane Lahrar, Patrice Simon, Céline Merlet. On the development of an original mesoscopic model to predict the capacitive properties of carbon-carbon supercapacitors. *Electrochimica Acta*, 2019, 327, pp.135022. 10.1016/j.electacta.2019.135022 . hal-02322514

HAL Id: hal-02322514

<https://hal.science/hal-02322514>

Submitted on 21 Oct 2019

HAL is a multi-disciplinary open access archive for the deposit and dissemination of scientific research documents, whether they are published or not. The documents may come from teaching and research institutions in France or abroad, or from public or private research centers.

L'archive ouverte pluridisciplinaire **HAL**, est destinée au dépôt et à la diffusion de documents scientifiques de niveau recherche, publiés ou non, émanant des établissements d'enseignement et de recherche français ou étrangers, des laboratoires publics ou privés.



On the development of an original mesoscopic model to predict the capacitive properties of carbon-carbon supercapacitors



Anouar Belhboub^{a, b}, El Hassane Lahrar^{a, b}, Patrice Simon^{a, b}, Céline Merlet^{a, b, *}

^a CIRIMAT, Université de Toulouse, CNRS, France

^b Réseau sur le Stockage Electrochimique de l'Énergie (RS2E), Fédération de Recherche CNRS, 3459, HUB de l'Énergie, Rue Baudelocque, 80039, Amiens, France

ARTICLE INFO

Article history:

Received 19 June 2019

Received in revised form

19 September 2019

Accepted 6 October 2019

Available online 11 October 2019

Keywords:

Lattice model

Supercapacitor

Nanoporous carbon

Solvation

Capacitance

ABSTRACT

We report on the development of a lattice model to predict structural, dynamical and capacitive properties of electrochemical double layer capacitors. The model uses input from molecular simulations, such as free energy profiles to describe the ion adsorption, and experiments, such as energy barriers for transitions between lattice sites. The model developed is approximately 10,000 times faster than common molecular simulations. We apply this model to a set of carbon structures with well-defined pore sizes and investigate the solvation effect by doing simulations with neat ionic liquids as well as acetonitrile-based electrolytes. We show that our model is able to predict quantities of adsorbed ions and capacitances in a range compatible with experimental values. We show that there is a strong dependency of the calculated properties on the pore size and on the presence or absence of solvent. In particular, for neat ionic liquids, larger capacitances are obtained for smaller pores, while the opposite trend is observed for organic electrolytes.

© 2019 The Authors. Published by Elsevier Ltd. This is an open access article under the CC BY-NC-ND license (<http://creativecommons.org/licenses/by-nc-nd/4.0/>).

1. Introduction

Carbon-carbon supercapacitors are electrochemical energy storage systems which store energy through ion adsorption at the interface between an electrolyte and porous carbon electrodes. Their high power density and long cycle life make them attractive for a number of applications in which they complement or sometimes even replace batteries. Supercapacitors are already used in applications such as regenerative energy braking [1] and catenary-free trams [2] where they are charged at every stop of the vehicle. Nevertheless, their relatively low energy density ($< 20 \text{ Wh kg}^{-1}$) compared to the one of batteries ($> 150 \text{ Wh kg}^{-1}$) [3,4] still limits their range of applications.

In 2006, there was a breakthrough in the field of supercapacitors when it was demonstrated that electrolyte ions could enter pores of subnanometer sizes leading to a large capacitance (and thus energy density) increase [5,6]. Since then, a number of experimental and theoretical projects have focused on understanding this capacitance increase and on designing new electrode materials with improved performances [7–13]. The molecular understanding of

the charge storage mechanisms is challenging due to the complex nature of the carbons and hence the difficulty to characterise them. Centeno et al. [14–16] proposed that the capacitance increase in carbon nanopores comes from incorrect measurements of the surface area of the porous carbons, but the confinement effect responsible for the improved charge storage in nanopores has been demonstrated using theoretical [12,17,18], including simulations with pores of very well defined accessible surfaces [19–21], and experimental studies [22], including the use of in-situ techniques [23,24]. While the capacitance increase is now well understood, reports of improvements in terms of capacitance are limited. Recent works report a capacitance of approximately 200 F g^{-1} in mesoporous [25] and pillared graphene [26] based supercapacitors.

One important issue in the field of supercapacitors is to assess the maximum capacitance that we could theoretically reach with an optimum system. Estimating a maximum capacitance in supercapacitors is a real challenge as it depends strongly on the ionic arrangements in the pores at a given potential which is the result of a large number of ion-ion and ion-electrode interactions. In supercapacitors, both the electrode and the electrolyte are disordered which makes them very difficult to characterise. A maximum value of 550 F g^{-1} , often quoted, was proposed by Xia et al. [27]. This capacitance is the one which would be obtained for a

* Corresponding author. CIRIMAT, Université de Toulouse, CNRS, France.
E-mail address: merlet@chimie.ups-tlse.fr (C. Merlet).

single layer of counterions on both sides of a graphene layer, more precisely located 0.3 nm away from the carbon surface. The small ion-carbon distance considered and the fact that a full charge-separation between counter- and co-ions is assumed suggest that this value cannot be reached. However, there is to-date, no better estimation for the maximum capacitance reachable in electrochemical double layer capacitors.

From a theoretical point of view, the most accurate approach to predict a capacitance is Molecular Dynamics simulations (MDs) because it allows one to describe the electrode-electrolyte interface microscopically [12,28]. One of the challenges associated with doing MDs of supercapacitors is to generate accurate atomistic models of the complex disordered carbons used in such systems. A number of ingenious strategies have been proposed in the past to obtain such disordered structures including Reverse Monte Carlo [29], Hybrid Reverse Monte Carlo [30,31], Quench Molecular Dynamics [32,33], and mimetic approaches related to experimental conditions [34,35]. The atomistic carbon structures generated in such ways are highly valuable as they allow one to probe microscopic phenomena at the molecular scale. However, this accuracy comes with the price of a high computational cost and a less straightforward characterisation compared to slit pore models [36,37] which prevents the use of MDs to realise a screening of porous carbons for supercapacitor applications.

Another issue with MDs is the small time and length scales which can be probed (a few nanoseconds, a few nanometers) usually far from the experimental values (a few micrometers at least, a few milliseconds or seconds). As such, the description of the carbon structure is usually not fully representative of the experimental reality, e.g. the pore size distributions of the model carbon electrodes are usually quite different from the experimental ones. Thus, in such systems, where phenomena on the atomistic scale have consequences on macroscopic length and timescales, it is important to develop new models to bridge the gap between molecular simulations and macroscopic values.

In this work, we report on the development of an original mesoscopic model to predict electrochemical performances of carbon-carbon supercapacitors at a much lower computational cost ($\sim 10^4 \times$ faster) than MD simulations. We adapt a lattice model which showed promising results for the simulation of ion diffusion and NMR spectra prediction for species adsorbed in neutral porous carbons [38,39]. Here, we implement new features to introduce the possibility of applying a potential to the modelled electrodes, and modify the way diffusion is treated in an attempt to get closer to reality. In the remainder of this article, we first describe the model before presenting the results obtained for two pure ionic liquids and two acetonitrile-based electrolytes in contact with a range of porous carbons having a simple pore size distribution (unimodal or bimodal). We study in particular the effects of solvation and pore size on the quantities of adsorbed ions and capacitive properties.

2. Description of the lattice gas model

In the lattice model, only one carbon electrode is simulated and its structure is represented as a cubic tridimensional set of interconnected discrete sites, separated by a lattice spacing, a . Each lattice site is an accessible space represented by a slit pore in the porous matrix. The lattice pores are characterised by i) a pore size, i.e. the width of the pore, and ii) a pore surface, corresponding to the lateral walls of the pore. The pore sizes are assigned randomly across the matrix according to pore size distributions (PSD) obtained experimentally or from atomistic structures of different types of carbons (microporous, mesoporous, ...). The pore surfaces are determined following a lognormal distribution with a mean value of -0.1 and a standard deviation of 0.25 (see Ref. [38] for a

detailed explanation of this choice).

In this study, we consider 10 different PSDs corresponding to atomistic structures reported by Deringer et al. [40], which were obtained by quench molecular dynamics using a machine learning based force field. These structures, with pore sizes ranging from 7 Å to 13 Å, are named GAP for the Gaussian Approximated Potential approach adopted for the force field. Fig. 1 shows the PSDs of the four GAP carbons discussed in the main text. Additional carbons with micropores in the same range of pore sizes were also considered to generate the electrode structures (see Fig. S1 in Supporting Information).

Once we have determined the structural features of the carbon lattice, we need to add a description of the adsorption profiles of the considered species. Thanks to its multi-scale nature, our lattice model can use data from molecular simulations, performed at the slit pore level, to represent the adsorption in our electrode-scale model. In this study, we use ionic densities from MDs to derive the integrated density of adsorbed ions of two tetrafluoroborate based electrolytes, the neat ionic liquid (IL) [BMI][BF₄] and the ACN-[BMI][BF₄] organic electrolyte (ACN stands for acetonitrile) and two hexafluorophosphate based electrolytes, [BMI][PF₆] and ACN-[BMI][PF₆], in contact with graphene-like electrodes [41]. The concentration of the acetonitrile-based electrolytes are equal to 1.5 M. In the main text, we focus on the BF₄-based electrolytes (the equivalent figures for the [BMI][PF₆]-based electrolytes are given in Supporting Information).

Figs. 2 and 3 give the integrated densities as a function of the pore size for BF₄⁻ anions and BMI⁺ cations in the organic electrolyte and neat ionic liquid. The adsorbed densities are calculated for the case of a zero potential difference ($\Delta V = 0$ V), as well as for applied potential differences of $\Delta V = 1, 1.5$ and 2 V.

From the integrated density profiles, we can see that, depending on their dimensions and on the potential applied, lattice sites are not identically populated. Therefore, each pore within the structure will have a different site energy E_i . This energy is equal to $E_i = -k_B T \ln(\rho_i)$, with ρ_i being the integrated density of site i , and conditions the lattice sites populations. To allow for ion diffusion between sites, we apply an acceptance rule to regulate inter-site transitions. The probability of a transition from site i to site j follows:

$$P(i,j) = \begin{cases} \exp\left(\frac{-(E_j - E_i)}{k_B T}\right) & \text{if } E_j > E_i \\ 1 & \text{if } E_j \leq E_i \end{cases} \quad (1)$$

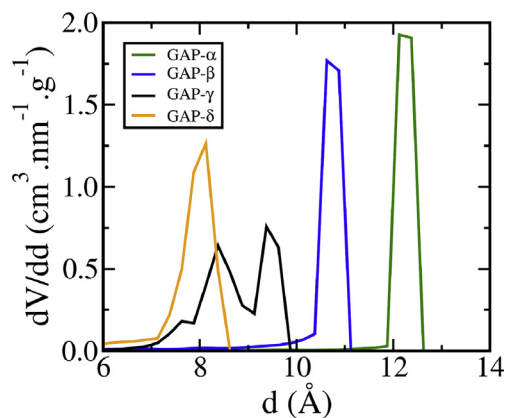


Fig. 1. Pore size distributions for the four carbons discussed in the main text, namely GAP- α , GAP- β , GAP- γ and GAP- δ , with average pore sizes $d_{\text{avg}} = 12.1, 10.5, 8.7$ and 7.7 Å, respectively.

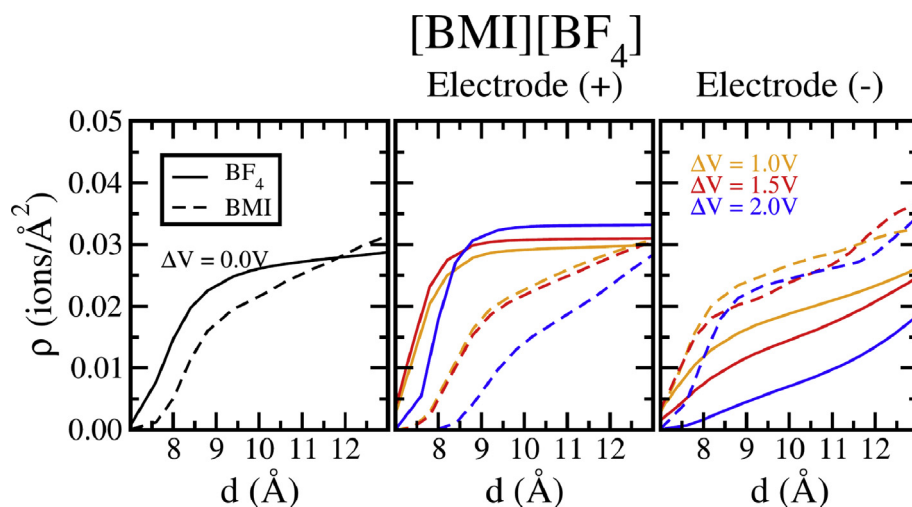


Fig. 2. Integrated density profiles of BF_4^- anions (solid lines) and BMI^+ cations (dashed lines) in the $[\text{BMI}][\text{BF}_4]$ neat IL as a function of pore size. The profiles are calculated for an applied potential difference of 0V, 1V, 1.5V and 2V.

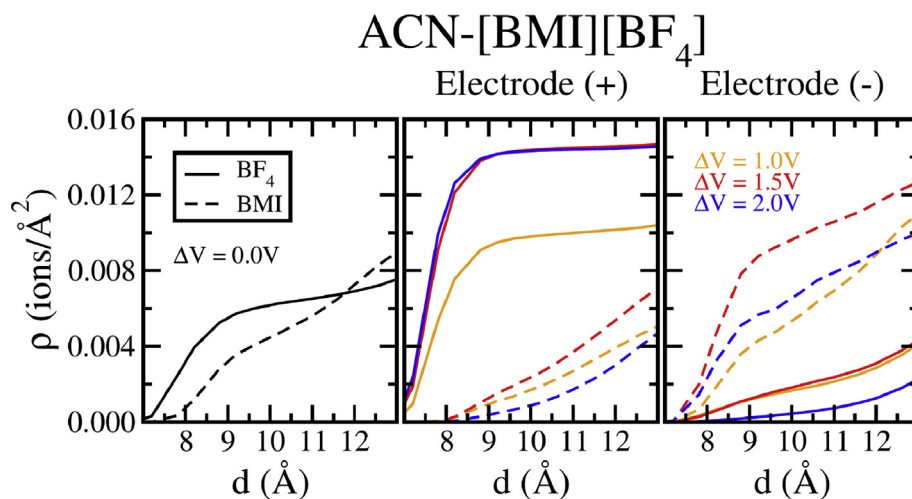


Fig. 3. Integrated density profiles of BF_4^- anions (solid lines) and BMI^+ cations (dashed lines) in the $\text{ACN}-[\text{BMI}][\text{BF}_4]$ organic electrolyte as a function of the pore size. The profiles are calculated for an applied potential difference of 0V, 1V, 1.5V and 2V.

This condition is defined to favor jumps from sites with higher energies to sites with lower energies. A transition from site i with higher energy to site j with lower energy will always occur, while the probability of the opposite jump will decrease as the difference $E_i - E_j$ increases.

To run a lattice model simulation, a number of iterations n and a timestep Δt are defined. For each iteration, particles are moved using the moment-propagation scheme [42–44], which is a recursive method allowing the examination of all possible trajectories at once and at a much lower computational cost than non-recursive methods. In the current state of the mesoscopic model, one calculation for a given system with 8,000 pores, i.e. corresponding to a $20 \times 20 \times 20$ cubic lattice, takes around 2–3 h on a single core. All simulations consist in an equilibration period (10,000 iterations), where the sites densities evolve towards their equilibrium values, and a production period (50,000 iterations), where the various properties are evaluated.

Inter-pore diffusion coefficients follow equation [38]:

$$D_{ij} = \alpha_{ij} \frac{a^2}{2d\Delta t} \quad (2)$$

where a is the lattice spacing and d is the dimensionality of the system. α_{ij} corresponds to a reduction factor for the inter-pore diffusion between two neighbouring lattice sites i and j compared to the bulk diffusion. This factor is defined as: $\alpha_{ij} = \exp\left(\frac{-E_a(ij)}{k_B T}\right)$, where $E_a(ij)$ is the energy barrier governing jumps between lattice sites i and j . The parametrisation of these energy barriers will be discussed in a later section.

3. Results and discussion

3.1. In-pore ion populations

To examine the validity of our model we first compare the total

in-pore ion populations, i.e. the sum of the number of adsorbed anions and the number of adsorbed cations $N_{in-pore} = N^{BF_4^-} + N^{BMI^+}$, calculated within the lattice model to the ones obtained in the framework of MD simulations. The details of the molecular simulations conducted are given in the Supporting Information. The comparison is done for all GAP electrodes in contact with neat [BMI][PF₆] at a 0 V potential difference. The total in-pore populations are plotted as a function of the average pore size of the GAP carbons (see Fig. 4). To ease the comparison between the lattice model and the molecular simulations results, the populations are normalised by the population of an arbitrarily chosen GAP carbon, here GAP-01 corresponding to $d_{avg} = 8.7 \text{ \AA}$. The population profile obtained from lattice model simulations presents similar features as the one of MD simulations but overestimates the quantities for the largest pore sizes. An interesting result is that the lattice model is able to reproduce the peaks of populations observed at around 8.7 \AA and 10.6 \AA . This shows that our model, which operates at the electrode scale, can grasp some of the microscopic characteristics of the considered porous carbon-based supercapacitors. The

overestimation could be due to the fact that our model underestimates the rugosity of the carbon structure, especially for pore interconnections. In the future, this could be improved by providing more accurate free energies on the lattice sites.

We now focus on the evolution of the total in-pore population when charging the electrode. Fig. 5 compares the adsorption profiles of the neat ionic liquid and the organic electrolyte in four carbon structures. The charge storage mechanism at the negative and positive electrodes involves adsorption of counter-ions and desorption of co-ions, i.e. ionic exchange, for both [BMI][BF₄] and ACN-[BMI][BF₄], and that for all the considered carbon types. The populations in the charged electrodes are normalised by the values at $\Delta V_0 = 0 \text{ V}$ to examine the evolution of adsorption/desorption mechanisms at non-zero applied potential differences. We see a clear dependency of the charge storage mechanisms on the pore size distributions, as well as on the absence/presence of solvent in the electrolyte. In general, when comparing carbons with different pore size distributions, we notice that higher ionic exchange occurs in carbons with smaller pores.

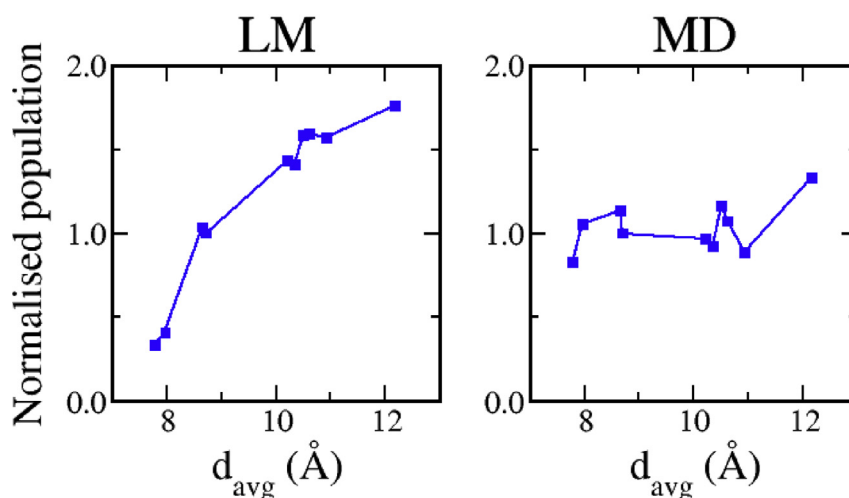


Fig. 4. Total in-pore population in GAP-based systems in contact with pure [BMI][PF₆]; comparison between the lattice model (LM) and Molecular Dynamics (MD) simulations. The calculations are carried out for an applied potential difference of 0 V. Populations are normalised by the GAP carbon with $d_{avg} = 8.7 \text{ \AA}$ (GAP-01 in the naming system of Deringer et al. [40]).

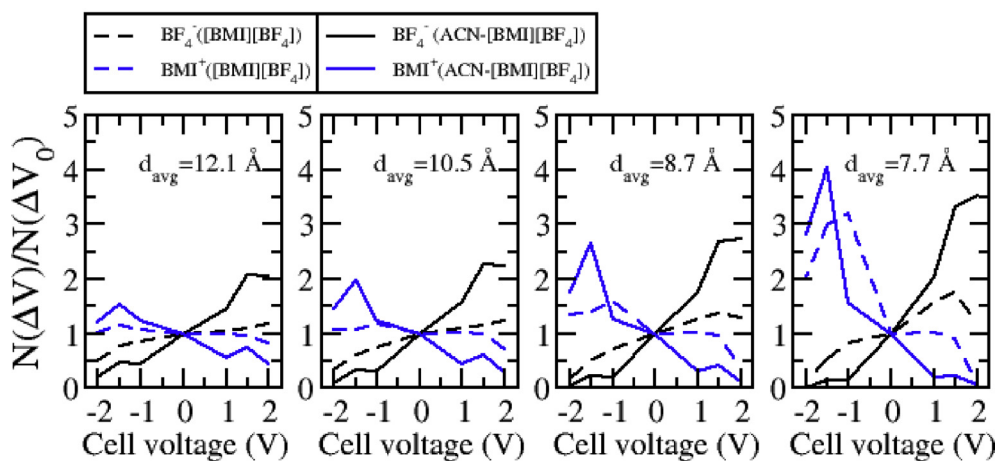


Fig. 5. Total in-pore ion population as a function of cell voltage for the considered electrode structures. Black and blue dashed lines show the populations of anions and cations, respectively, in the neat IL. Black and blue solid lines show the populations of anions and cations, respectively, in the organic electrolyte. Anions and cations populations are normalised by their equivalents at $\Delta V_0 = 0 \text{ V}$. The voltages indicated correspond to the full cell voltage, e.g. 2 V (respectively -2 V) designates the positive electrode (respectively the negative electrode) for a 2 V potential difference. (For interpretation of the references to colour in this figure legend, the reader is referred to the Web version of this article.)

To characterise more precisely the relative importance of adsorption/desorption, we define the ionic exchange ratio as follows:

$$\alpha_{\text{exchange}} = \left| \frac{N^{\text{BF}_4}(\Delta V)}{N^{\text{BF}_4}(\Delta V_0)} - \frac{N^{\text{BMI}}(\Delta V)}{N^{\text{BMI}}(\Delta V_0)} \right| \quad (3)$$

This quantity is similar to the charging mechanism parameter [45,46] and the charge efficiency [47–50] proposed in other works. Fig. 6 shows the ionic exchange ratio α_{exchange} as a function of the average pore sizes of the carbons. For neat [BMI][BF₄], in addition to the decrease of ionic exchange for carbons with larger pore sizes, we notice that this mechanism is more pronounced at the negative electrode, compared to the positive one. This is observed for all the considered applied potentials (i.e. $\Delta V = 1$ V, 1.5 V and 2 V). Since the anions and cations have different sizes, shapes and charge distributions, it is not surprising to observe an asymmetry between the positive and negative electrodes. The difference in mechanisms could be explained by a higher mobility of BMI⁺ cations [51]. At the negative electrode, applying a potential difference leads to the insertion of an important quantity of cations therefore forcing more BF₄⁻ anions to exit the carbons micropores. This is clear at small pore sizes but not seen at larger pore sizes for which the relative differences between 0 V and a non-zero potential difference are smaller. In contrast, at the positive electrode, the large desorption of BMI⁺ cations is accompanied by a less important adsorption of BF₄⁻ anions in the considered voltage range, leading to a smaller ionic exchange. Again, this effect depends on the pore size as the large size of the cation probably leads to larger steric effects in the smallest pores.

Adding a solvent, here acetonitrile, to the IL greatly changes the profile of the in-pore ions adsorption. In this case, the solvent screens the electrostatic coupling between ions and increases the mobility of anions and cations within carbons pores. The solvent also stabilises the ions leading to an easier charge separation. This results in a notable increase of the ionic exchange, reaching in some cases three times the value of that of the neat IL. The solvent addition also introduces changes of the ionic orientations. This combined with the screening induced enhancement of ion mobility, which favors BF₄⁻ anions in this case [51], influences the asymmetric character of the ionic exchange. In this case, the

exchange ratio tends to be higher at the positive electrode, as opposed to the previous case of the neat IL. These results are consistent with Electrochemical Quartz Crystal Microbalance experiments done on the [EMI][TFSI]-ACN electrolyte (1-ethyl-3-methylimidazolium bis(trifluoromethanesulfonyl)imide) [52].

We note here that the calculations carried out for the 6 additional carbon structures and the [BMI][PF₆]-based electrolytes give similar results (see Figs. S4–S9 in Supporting Information). Moreover, the effect of the solvation leading to an increase of the ionic exchange was also observed in molecular simulations as described in Table S1 of the Supporting Information.

3.2. Capacitive properties

We pointed out that the charge storage mechanism involved simultaneous counter-ion adsorption and co-ion desorption in the carbon micropores. We now focus on the impact of the variations in ionic exchange on the capacitive properties of the electrodes considered. We calculate the absolute value of the total ionic charge stored in the electrode as:

$$Q^{\text{ionic}} = |N^{\text{BF}_4} - N^{\text{BMI}}| e \quad (4)$$

where N^{BF_4} and N^{BMI} are the in-pore populations of anions and cations, respectively, and e is the elementary charge.

Fig. 7 shows the calculated ionic charges for the considered carbon structures in contact with the neat IL and the organic electrolyte. The ionic charges normalised by the total surface area give values in the range of reported experimental data [5,53]. We note that lattice simulations give non-zero stored charges at $\Delta V = 0$ V. This results from the integrated ionic density profiles (see Figs. 2 and 3) extracted from MDs of electrolytes confined in larger slit pores than the pore sizes considered here. This is one aspect of the model which requires improvements, out of the scope of the current work, in order to give more realistic results.

In general, systems containing the neat IL store considerably more charge than the ones with the organic electrolyte. This is surprising knowing that the ionic exchange is more important using ACN-[BMI][BF₄]. However, the absolute numbers of adsorbed ions within the micropores are much larger in the neat IL than in the organic electrolyte (see Table S2 in Supporting information). This can explain, at least partially, the higher ionic charge in the neat IL. Moreover, for $\Delta V = 0$ V, all carbon structures have a higher initial charge for the neat IL compared to the solvated electrolyte. Therefore, even though the ratio of exchange is higher when charging the system containing the organic electrolyte, the higher initial charge for [BMI][BF₄] gives this electrolyte an advantage.

The carbons with smaller micropores, i.e. GAP- γ and GAP- δ , further illustrate this trend. Indeed, for these structures the difference between [BMI][BF₄] and ACN-[BMI][BF₄] in the charge stored at $\Delta V = 0$ V is much higher than for GAP- α and GAP- β . Upon charging, this difference is retained and a higher charge is stored for [BMI][BF₄] in contact with both the positive and negative electrode. For GAP- α and GAP- β , the smaller difference in charge storage at $\Delta V = 0$ V is rapidly overtaken by the more pronounced ionic exchange in the organic electrolyte, which appears to be dominant at the positive electrode. As a result, a higher charge is stored at the interface between the positive electrode and ACN-[BMI][BF₄].

From the obtained ionic charge we can calculate the capacitance of each electrode as: $C_{\pm} = Q_{\pm}^{\text{ionic}} / \Delta V_{\pm}$, with C_{+} and C_{-} representing the capacitances of the positive and negative electrode, respectively. C_{+} and C_{-} as a function of ΔV_{+} and ΔV_{-} , respectively, are given in Fig. S10 in the Supporting Information. The values for ΔV_{\pm} , i.e. the potential drops at the electrode-electrolyte interface, are

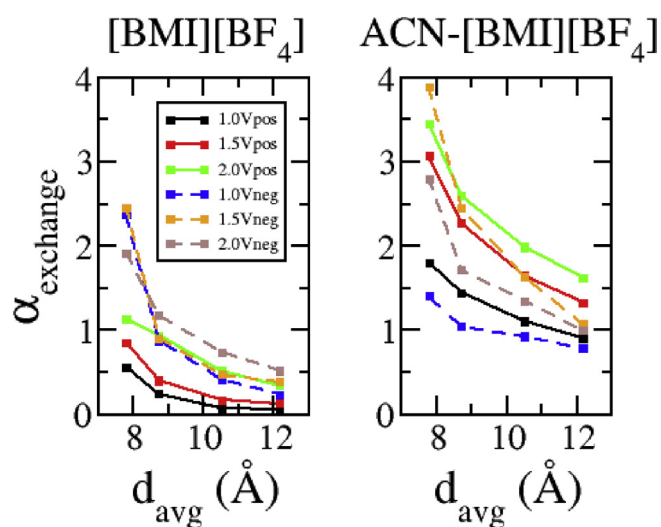


Fig. 6. Ionic exchange α_{exchange} as a function of the average pore size of the porous carbon structures. The exchange is calculated at the positive and negative electrodes for the considered applied potential differences.

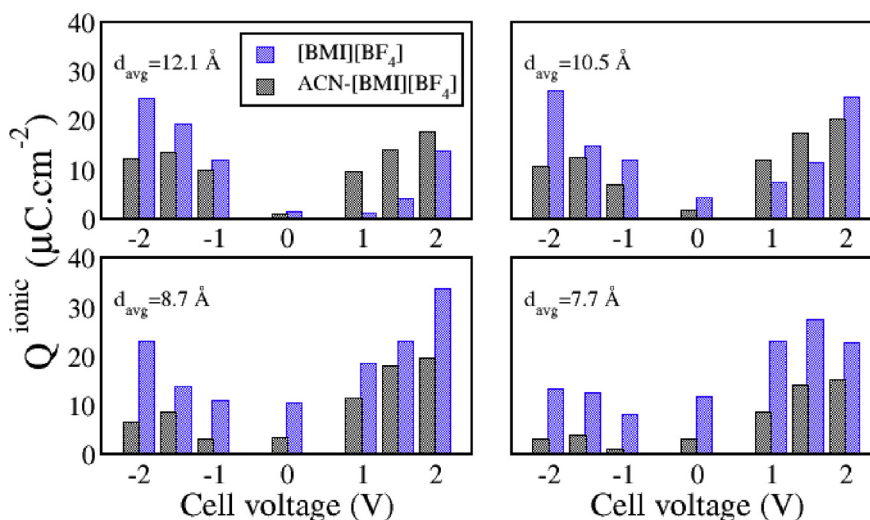


Fig. 7. Ionic charges stored at the positive and negative electrodes for the considered porous carbons. Blue and black bars give the charges obtained considering the neat IL and the organic electrolyte, respectively. The calculated ionic charges are normalised by the total electrode surface. The voltages indicated correspond to the full cell voltage, e.g. 2 V (respectively -2 V) designates the positive electrode (respectively the negative electrode) for a 2 V potential difference. (For interpretation of the references to colour in this figure legend, the reader is referred to the Web version of this article.)

taken from MD simulations previously reported [41]. We note that the same trends are obtained if we simply take $\Delta V_+ = \Delta V_- = \Delta V / 2$. Fig. 8 shows the total capacitance of the considered systems as a function of the applied potential difference. The total capacitance is calculated as:

$$\frac{1}{C} = \frac{1}{C_+} + \frac{1}{C_-} \quad (5)$$

We clearly see that the performance of the overall system is greatly influenced both by the carbon structure and the presence of solvent. When the electrode structure contains smaller pores, it shows better performances when in contact with the neat IL as the capacitance values in this case are clearly higher than the ones obtained with the organic electrolyte. As an example, for an applied potential difference of $\Delta V = 1$ V, GAP- γ - and GAP- δ -based systems ($d_{\text{avg}} = 8.7$ Å and $d_{\text{avg}} = 7.7$ Å, respectively) have a capacitance of 12.71 and 11.15 $\mu\text{F cm}^{-2}$, respectively, when the system contains [BMI][BF₄], compared to 4.64 and 1.71 $\mu\text{F cm}^{-2}$ for the ACN-[BMI][BF₄]-based systems. In contrast, the solvent addition improves the storage mechanism when the electrode contains larger pores. If we

take the same case of $\Delta V = 1$ V, we see that GAP- α -based system ($d_{\text{avg}} = 12.1$ Å) present a higher capacitance for ACN-[BMI][BF₄] (9.08 $\mu\text{F cm}^{-2}$) than for [BMI][BF₄] (2.04 $\mu\text{F cm}^{-2}$). For GAP- β ($d_{\text{avg}} = 10.5$ Å) the capacitive performance is improved when the system contains the organic electrolyte. Indeed, the difference in capacitance using ACN-[BMI][BF₄] and [BMI][BF₄] is considerably smaller (i.e. 7.92 $\mu\text{F cm}^{-2}$ for ACN-[BMI][BF₄] and 8.42 $\mu\text{F cm}^{-2}$ for [BMI][BF₄]), compared to the case of the electrode structure containing mainly small micropores.

It is quite surprising that the neat IL and the organic electrolyte give opposite variations with the pore size as this is not what is observed experimentally [5,53]. One of the reason for this discrepancy could be the fact that in our lattice model, we represent only one electrode and as such, there is no interplay between the negative and positive electrodes which usually leads to one electrode being limiting in terms of charge storage. The difference in the stored ionic charges is an artefact of our model and is experimentally unrealistic in a two-electrode system. Strategies to overcome this limitation will be explored in a future work but comparisons with three-electrode systems might still be valid with

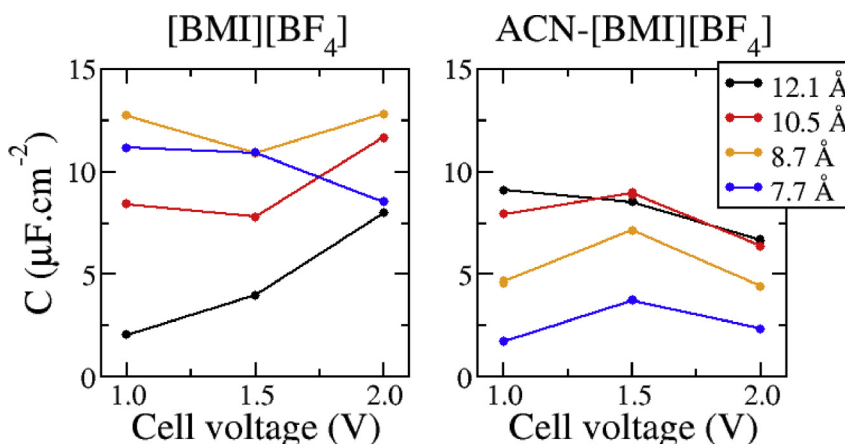


Fig. 8. Total capacitance as a function of the applied potential difference obtained for [BMI][BF₄] and ACN-[BMI][BF₄] in contact with GAP- α , GAP- β , GAP- γ and GAP- δ . Capacitances are normalised by the total electrode surface.

our approach. Another reason for the unexpected variation with pore size could be the inaccuracy of the free energy profiles, this can be checked in future works by implementing a better description of these adsorption profiles. Finally, the experimental carbons are actually much more disordered than the carbons studied here, it is thus possible that such an effect would be observed in carbons with well defined pore sizes.

3.3. Diffusion

As mentioned before, the diffusion coefficients of the ions and solvent molecules in the lattice depend on the energy barriers between lattice sites, which are unknown. In previous works these energy barriers were assigned following a Gaussian distribution to calculate diffusion and NMR spectra in porous carbons [38]. However, this description lacks a dependency on the structural properties of the pores and of the adsorbed species. To overcome this, we now calculate energy barriers in order to reproduce experimental trends showing that diffusion coefficients decrease as the total in-pore population within the carbon structures increases [54].

The energy barriers considered to calculate the diffusion coefficients are fitted (using an exponential function) on the experimental data to reproduce the experimental dependence of diffusion on the in-pore populations. Figs. 9 and 10 show the resulting diffusion coefficients as a function of average pore sizes for various potentials. Data shown in Figs. S11 and S12 in the Supporting Information confirm that the energy barriers assigned allow us to reproduce the exponential decay with in-pore populations.

We now focus on the relationship between diffusion and structural properties of the considered carbon structures. Figs. 9 and 10 give the diffusion coefficients (normalised by the bulk diffusion, $D_0 = \frac{a^2}{2d\Delta t}$) as a function of the average pore sizes of the carbons for BF_4^- and BMI^+ in $[\text{BMI}][\text{BF}_4]$ and $\text{ACN}-[\text{BMI}][\text{BF}_4]$ for all the considered applied potential differences.

In systems containing the organic electrolyte (Fig. 9), we notice that diffusion tends to decrease in carbons with larger micropores for both anions and cations. Moreover, diffusion of a given ion type seems to occur at the same rate within both the positive and negative electrode. This dependency is in line with the ionic

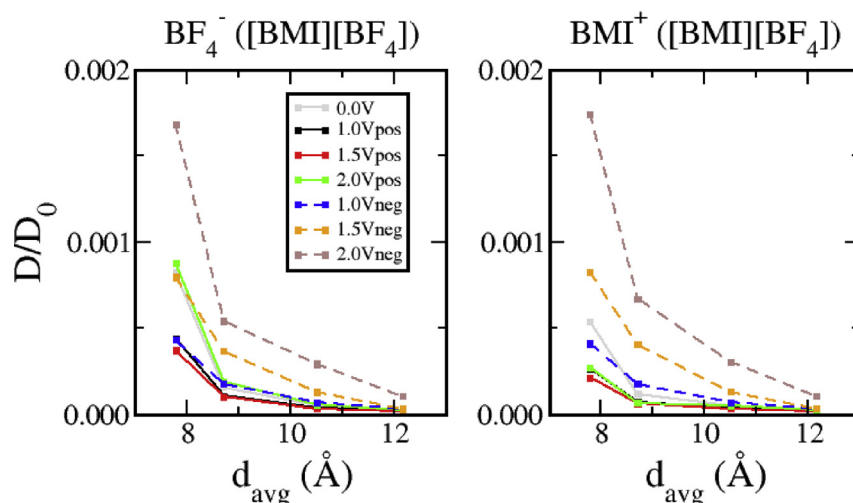


Fig. 9. Diffusion coefficients of adsorbed BF_4^- anions and BMI^+ cations as a function of average pore size in systems containing the neat IL. Calculations are obtained for $\Delta V = 0, 1, 1.5$ and 2V .

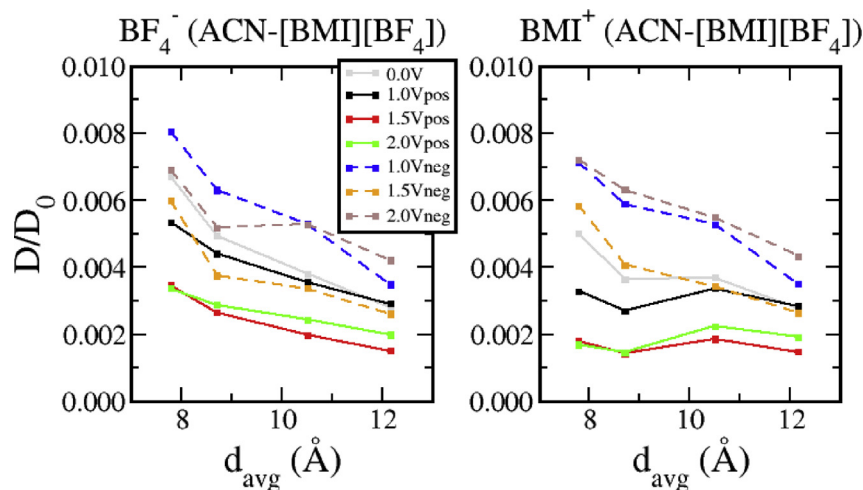


Fig. 10. Diffusion coefficients of adsorbed BF_4^- anions and BMI^+ cations as a function of average pore size in systems containing the organic electrolyte. Results are shown for $\Delta V = 0, 1, 1.5$ and 2V .

exchange profiles. When the pore size increases, the decay in diffusion is accompanied by a less dominant ionic exchange mechanism. The same dependencies are obtained when carbons are in contact with the neat IL (Fig. 10), as the decrease of diffusion coefficients of BF_4^- anions and BMI^+ cations is even more pronounced when considering carbons with larger micropores.

Additionally, the solvation tends to amplify the inter-pore diffusion. Indeed, diffusion coefficients of anions and cations are almost one order of magnitude larger in systems with organic electrolyte compared to the ones with the neat IL. This is understandable knowing that solvation reduces the electrostatic coupling between ion pairs and the interaction of ions with pores walls. Moreover, this amplification of the diffusion induced by the solvation effect is also in agreement with the ionic exchange data, as we noted that the exchange mechanism is more dominant when considering the organic electrolyte compared to the neat IL. Finally, we remind that the dependencies discussed above were validated considering additional carbon structures and electrolyte compositions (see Figs. S13 and S14 in the Supporting Information).

While the results obtained are consistent with our assignment of energy barriers, it is worth noting that we obtain larger diffusion coefficients for smaller pore sizes which is unexpected. Actually, the experimental results of Forse et al. [54] were obtained for a single carbon type and a single electrolyte. It is possible that the trend observed is not valid across a range of carbons. The current model only links diffusion to ionic in-pore populations and it is clear that a more complete description will take into account additional aspects related to the structural properties of the porous matrix, which is a complicated task to perform. A very recent theoretical work, based on MDs with slit pores of various widths, showed an opposite trend of diffusion as a function of pore sizes [55]. However, it is worth noting that those calculations were performed for a larger range of pore sizes than the current study, and that the trend is not monotonous in the interval of pore sizes similar to the one considered in this work (i.e. around 10 Å). Work is ongoing to parametrise the variation of energy barriers across various pore sizes and shapes using molecular simulations results.

4. Conclusions

In this work, we report on the development and application of a mesoscopic lattice model used to study the relationship between structural and capacitive properties in porous carbon-based supercapacitors. This type of model was chosen for its high computational efficiency and we estimate that it is 10,000 times faster than molecular simulations. Several supercapacitor models were examined by considering various microporous carbon structures and electrolytes. In particular, the solvent effect was investigated by considering neat ILs, namely $[\text{BMI}][\text{BF}_4]$ and $[\text{BMI}][\text{PF}_6]$, and their acetonitrile-solvated equivalents.

We showed that all systems exhibit ionic exchange upon charging the electrodes. This exchange appeared to be less important in carbon structures having large micropores, and more marked for organic electrolytes compared to neat ILs. The diffusion coefficients calculated follow this change of mechanism, with the decrease of diffusion coefficients in larger micropores and in neat ILs (compared to organic electrolytes). The lattice model also showed the effect of solvation on the charge storage in porous carbon-based supercapacitors. Even though ions exhibit higher exchange in organic electrolytes, the larger absolute numbers of adsorbed ions for neat ILs result in more charge storage for these systems. Moreover, the model showed that the capacitance tends to be higher in systems combining neat ILs or organic electrolytes with carbons containing mainly small or large micropores,

respectively.

In summary, our results show that the lattice model is able to retain some microscopic information and predict quantities of adsorbed ions, capacitances and diffusion coefficients in an efficient manner. However, for the lattice model to become suitable for a systematic study of the structural and dynamical properties of carbon-carbon supercapacitors, it is clear that further improvements are needed to better describe the microscopic information used as input. In particular the free energy profiles describing the ion adsorption and the energy barriers for diffusion. For instance, using data from molecular simulations performed on porous electrode structures, instead of the graphene-like systems considered here, could considerably improve the accuracy of the model. Other perspectives include the description of the free energy profiles through a classical density functional theory approach in order to remove the need for molecular simulations.

5. Data availability

The data corresponding to the plots reported in this paper (pore size distributions, integrated densities, in-pore populations, ionic exchange values, capacitances, ionic charges and diffusion coefficients) are available in the Zenodo repository with identifier 10.5281/zenodo.3250139.

Declaration of competing interest

The authors declare no competing interest.

Acknowledgments

This project has received funding from the European Research Council (ERC) under the European Union's Horizon 2020 research and innovation programme (grant agreement no. 714581). This work was granted access to the HPC resources of CALMIP supercomputing center under the allocation P17037.

Appendix A. Supplementary data

Supplementary data to this article can be found online at <https://doi.org/10.1016/j.electacta.2019.135022>.

References

- [1] Y. Yoshida, H.P. Figueroa, R.A. Dougal, Comparison of energy storage configurations in railway microgrids, 2017, in: *IEEE Second International Conference on DC Microgrids (ICDCM)*, 2017, pp. 133–138.
- [2] Y. Zhang, Z. Wei, H. Li, L. Cai, J. Pan, Optimal charging scheduling for catenary-free trams in public transportation systems, *IEEE Trans. Smart Grid* 10 (2019) 227–237.
- [3] P. Simon, Y. Gogotsi, Materials for electrochemical capacitors, *Nat. Mater.* 7 (2008) 845–854.
- [4] B.Y. Guan, A. Kushima, L. Yu, S. Li, J. Li, X.W.D. Lou, Coordination polymers derived general synthesis of multishelled mixed metal-oxide particles for hybrid supercapacitors, *Adv. Mater.* 29 (2017) 1605902.
- [5] J. Chmiola, G. Yushin, Y. Gogotsi, C. Portet, P. Simon, P.L. Taberna, Anomalous increase in carbon capacitance at pore sizes less than 1 nanometer, *Science* 313 (2006) 1760–1763.
- [6] E. Raymundo-Piñero, K. Kierzek, J. Machnikowski, F. Béguin, Relationship between the nanoporous texture of activated carbons and their capacitance properties in different electrolytes, *Carbon* 44 (2006) 2498–2507.
- [7] D. Sheberla, J.C. Bachman, J.S. Elias, C.-J. Sun, Y. Shao-Horn, M. Dincă, Conductive MOF electrodes for stable supercapacitors with high areal capacitance, *Nat. Mater.* 16 (2017) 220–224.
- [8] Y. Zhu, S. Murali, M.D. Stoller, K.J. Ganesh, W. Cai, P.J. Ferreira, A. Pirkle, R.M. Wallace, K.A. Cychoz, M. Thommes, D. Su, E.A. Stach, R.S. Ruoff, Carbon-based supercapacitors produced by activation of graphene, *Science* 332 (2011) 1537–1541.
- [9] L.L. Zhang, X.S. Zhao, Carbon-based materials as supercapacitor electrodes, *Chem. Soc. Rev.* 38 (2009) 2520–2531.
- [10] Y. Tao, X. Xie, W. Lu, D.-M. Tang, D. Kong, Z. Huang, H. Nishihara, T. Ishii, B. Li,

- D. Golberg, F. Kang, T. Kyotani, Q.-H. Yang, Towards ultrahigh volumetric capacitance: graphene derived highly dense but porous carbons for supercapacitors, *Sci. Rep.* 3 (2013) 2975.
- [11] P. Simon, Y. Gogotsi, Capacitive energy storage in nanostructured carbon–electrolyte systems, *Acc. Chem. Res.* 46 (2013) 1094–1103.
- [12] C. Merlet, B. Rotenberg, P.A. Madden, P.-L. Taberna, P. Simon, Y. Gogotsi, M. Salanne, On the molecular origin of supercapacitance in nanoporous carbon electrodes, *Nat. Mater.* 11 (2012) 306–310.
- [13] Q. Liao, N. Li, S. Jin, G. Yang, C. Wang, All-solid-state symmetric supercapacitor based on Co_3O_4 nanoparticles on vertically aligned graphene, *ACS Nano* 9 (2015) 5310–5317.
- [14] T.A. Centeno, O. Sereda, F. Stoeckli, Capacitance in carbon pores of 0.7 to 15 nm: a regular pattern, *Phys. Chem. Chem. Phys.* 13 (2011) 12403–12406.
- [15] F. Stoeckli, T.A. Centeno, Pore size distribution and capacitance in microporous carbons, *Phys. Chem. Chem. Phys.* 14 (2012) 11589–11591.
- [16] A. García-Gómez, G. Moreno-Fernández, B. Lobato, T.A. Centeno, Constant capacitance in nanopores of carbon monoliths, *Phys. Chem. Chem. Phys.* 17 (2015).
- [17] C. Merlet, C. Péan, B. Rotenberg, P.A. Madden, B. Daffos, P.L. Taberna, P. Simon, M. Salanne, Highly confined ions store charge more efficiently in supercapacitors, *Nat. Commun.* 4 (2013a) 2701.
- [18] M. Salanne, B. Rotenberg, K. Naoi, K. Kaneko, P.-L. Taberna, C.P. Grey, B. Dunn, P. Simon, Efficient storage mechanisms for building better supercapacitors, *Nature Energy* 1 (2016) 16070.
- [19] G. Feng, P.T. Cummings, Supercapacitor capacitance exhibits oscillatory behavior as a function of nanopore size, *J. Phys. Chem. Lett.* 2 (2011a) 2859–2864.
- [20] P. Wu, J. Huang, V. Meunier, B.G. Sumpter, R. Qiao, Complex capacitance scaling in ionic liquids-filled nanopores, *ACS Nano* 5 (2011) 9044–9051.
- [21] D. Jiang, Z. Jin, J. Wu, Oscillation of capacitance inside nanopores, *Nano Lett.* 11 (2011) 5373–5377.
- [22] N. Jäckel, P. Simon, Y. Gogotsi, V. Presser, Increase in capacitance by sub-nanometer pores in carbon, *ACS Energy Lett.* 1 (2016) 1262.
- [23] D.T.L. Gallena, B.C. Bayer, S. Hofmann, G.A.J. Amaratunga, Understanding capacitance variation in sub-nanometer pores by *in situ* tuning of interlayer constrictions, *ACS Nano* 10 (2016) 747–754.
- [24] C. Prehal, C. Koczwarra, N. Jäckel, A. Schreiber, M. Burian, H. Amenitsch, M.A. Hartmann, V. Presser, O. Paris, Quantification of ion confinement and desolvation in nanoporous carbon supercapacitors with modelling and *in situ* X-ray scattering, *Nature Energy* 2 (2017) 16215.
- [25] J. Liu, W. Li, D. Zhao, Mesoporous materials for energy conversion and storage devices, *Nat. Rev. Mater.* 1 (2016) 16023.
- [26] H. Banda, S. Périé, B. Daffos, P.-L. Taberna, L. Dubois, O. Crosnier, P. Simon, D. Lee, G. De Paëpe, F. Duclairoir, Sparsely pillared graphene materials for high-performance supercapacitors: improving ion transport and storage capacity, *ACS Nano* 13 (2019) 1443–1453.
- [27] J. Xia, F. Chen, J. Li, N. Tao, Measurement of the quantum capacitance of graphene, *Nat. Nanotechnol.* 4 (2009) 505–509.
- [28] G. Feng, P.T. Cummings, Supercapacitor capacitance exhibits oscillatory behavior as a function of nanopore size, *J. Phys. Chem. Lett.* 2 (2011b) 2859–2864.
- [29] K. Thomson, K.E. Gubbins, Modeling structural morphology of microporous carbons by Reverse Monte Carlo, *Langmuir* 16 (2000) 5761–5773.
- [30] A.H. Farmahini, G. Opletal, S.K. Bhatia, Structural modelling of silicon carbide-derived nanoporous carbon by Hybrid Reverse Monte Carlo simulation, *J. Phys. Chem. C* 117 (2013) 14081–14094.
- [31] J.C. Palmer, S.J. Jain, K.E. Gubbins, N. Cohaut, J.E. Fischer, R.K. Dash, Y. Gogotsi, Hybrid Reverse Monte Carlo simulations of microporous carbons. Royal society of chemistry, Characterisation of Porous Solids vol. III, in: Proceedings of the 8th International Symposium on the Characterisation of Porous Solids, 2009.
- [32] J.C. Palmer, A. Lobet, S.-H. Yeon, J.E. Fischer, Y. Shi, Y. Gogotsi, K.E. Gubbins, Modeling the structural evolution of carbide-derived carbons using quenched molecular dynamics, *Carbon* 48 (2010) 1116–1123.
- [33] M.W. Thompson, B. Dyatkin, H.-W. Wang, C.H. Turner, X. Sang, R.R. Unocic, C.R. Iacovella, Y. Gogotsi, A.C.T. van Duin, P.T. Cummings, An atomistic carbide-derived carbon model generated using ReaxFF-based quenched molecular dynamics, *C J. Carbon Res.* 3 (2017) 32.
- [34] C. de Tomas, I. Suarez-Martinez, F. Vallejós-Burgos, M.J. López, K. Kaneko, N.A. Marks, Structural prediction of graphitization and porosity in carbide-derived carbons, *Carbon* 119 (1) (2017).
- [35] S. Schweizer, R. Meißner, M. Amkreutz, K. Thiel, P. Schiffels, J. Landwehr, B.J.M. Etzold, J.-R. Hill, Molecular modeling of microporous structures of carbide-derived carbon-based supercapacitors, *J. Phys. Chem. C* 121 (2017) 7221–7231.
- [36] S.K. Bhatia, Characterizing structural complexity in disordered carbons: from the slit pore to atomistic models, *Langmuir* 33 (2017) 831–847.
- [37] A.H. Farmahini, S.K. Bhatia, Hybrid Reverse Monte Carlo simulation of amorphous carbon: distinguishing between competing structures obtained using different modeling protocols, *Carbon* 83 (2015) 53–70.
- [38] C. Merlet, A.C. Forse, J.M. Griffin, D. Frenkel, C.P. Grey, Lattice simulation method to model diffusion and NMR spectra in porous materials, *J. Chem. Phys.* 142 (2015), 094701.
- [39] A.C. Forse, C. Merlet, P.K. Allan, E.K. Humphreys, J.M. Griffin, M. Aslan, M. Zeiger, V. Presser, Y. Gogotsi, C.P. Grey, New insights into the structure of nanoporous carbons from NMR, Raman, and pair distribution function analysis, *Chem. Mater.* 27 (2015) 6848–6857.
- [40] V.L. Deringer, C. Merlet, Y. Hu, T.H. Lee, J.A. Kattirtzi, O. Pecher, G. Csányi, S.R. Elliott, C.P. Grey, Towards an atomistic understanding of disordered carbon electrode materials, *Chem. Commun.* 54 (2018) 5988–5991.
- [41] C. Merlet, M. Salanne, B. Rotenberg, P.A. Madden, Influence of solvation on the structural and capacitive properties of electrical double layer capacitors, *Electrochim. Acta* 101 (2013b) 262–271.
- [42] D. Frenkel, Velocity auto-correlation functions in a 2D lattice lorentz gas: comparison of theory and computer simulation, *Phys. Lett. A* 121 (1987) 385–389.
- [43] M. Levesque, M. Duval, I. Pagonabarraga, D. Frenkel, B. Rotenberg, Accounting for adsorption and desorption in lattice Boltzmann simulations, *Phys. Rev. E* 88 (2013), 013308.
- [44] B. Rotenberg, I. Pagonabarraga, D. Frenkel, Dispersion of charged tracers in charged porous media, *Europhys. Lett.* 83 (2008) 34004.
- [45] A.C. Forse, C. Merlet, J.M. Griffin, C.P. Grey, New perspectives on the charging mechanisms of supercapacitors, *J. Am. Chem. Soc.* 138 (2016) 5731–5744.
- [46] C. Prehal, C. Koczwarra, H. Amenitsch, V. Presser, O. Paris, Salt concentration and charging velocity determine ion charge storage mechanism in nanoporous supercapacitors, *Nat. Commun.* 9 (2018) 4145.
- [47] R. Zhao, P.M. Biesheuvel, H. Miedema, H. Bruning, A. van der Wal, Charge efficiency: a functional tool to probe the double-layer structure inside of porous electrodes and application in the modeling of capacitive deionization, *J. Phys. Chem. Lett.* 1 (2010) 205–210.
- [48] E. Avraham, M. Noked, Y. Bouhadana, A. Soffer, D. Aurbach, Limitations of charge efficiency in capacitive deionization. II. On the behavior of CDI cells comprising two activated carbon electrodes, *J. Electrochem. Soc.* 156 (2009) 157–162.
- [49] P.M. Biesheuvel, S. Porada, M. Levi, M.Z. Bazant, Attractive forces in microporous carbon electrodes for capacitive deionization, *J. Solid State Electrochem.* 18 (2014) 1365–1376.
- [50] T. Kim, J.E. Dykstra, S. Porada, A. van der Wal, J. Yoon, P.M. Biesheuvel, Enhanced charge efficiency and reduced energy use in capacitive deionization by increasing the discharge voltage, *J. Colloid Interface Sci.* 446 (2015) 317–326.
- [51] C. Merlet, Modélisation de l'adsorption des ions dans les carbones nanoporeux, PhD thesis, Université Pierre et Marie Curie, 2013.
- [52] W.-Y. Tsai, P.-L. Taberna, P. Simon, Electrochemical quartz crystal microbalance (EQCM) study of ion dynamics in nanoporous carbons, *J. Am. Chem. Soc.* 136 (2014) 8722–8728.
- [53] C. Largeot, C. Portet, J. Chmiola, P.-L. Taberna, Y. Gogotsi, P. Simon, Relation between the ion size and pore size for an electric double-layer capacitor, *J. Am. Chem. Soc.* 130 (2008) 2730–2731.
- [54] A.C. Forse, J.M. Griffin, C. Merlet, J. Carreteo-Gonzalez, A.-R.O. Raji, N.M. Trease, C.P. Grey, Direct observation of ion dynamics in supercapacitor electrodes using *in situ* diffusion NMR spectroscopy, *Nature Energy* 2 (2017) 16216.
- [55] C. Wang, Y. Wang, Y. Lu, H. He, F. Huo, K. Dong, N. Wei, S. Zhang, Height-driven structure and thermodynamic properties of confined ionic liquids inside carbon nanochannels from molecular dynamics study, *Phys. Chem. Chem. Phys.* 21 (2019) 12767–12776.